Available online at www.sciencedirect.com

ScienceDirect

journal homepage: www.elsevier.com/locate/he

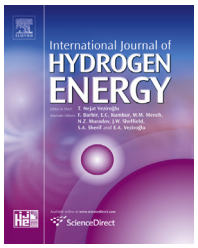

Mg–M–LiH alloys prepared by mechanical milling and their hydrogen storage characteristics

K. Suárez-Alcántara [a,*], A.F. Palacios-Lazcano [b], T. Funatsu [c], J.G. Cabañas-Moreno [d]

[a] Unidad Morelia del Instituto de Investigaciones en Materiales, Universidad Nacional Autónoma de México, Antigua carretera a Pátzcuaro 8701, Col. Ex-hacienda de San José de la Huerta, Morelia, Michoacán, 58190, Mexico
[b] ESIME Zacatenco, Av. Luis Enrique Erro S/N, Unidad Profesional Adolfo López Mateos, Zacatenco, Delegación Gustavo A. Madero, Distrito Federal, 07738, Mexico
[c] Techno System CO., LTD, Karasakinaka 3-1-1, Takatsuki-City, Osaka, Japan
[d] Centro de Investigación y de Estudios Avanzados, IPN, Av. Instituto Politécnico Nacional 2508, México, D. F., 07360, Mexico

ARTICLE INFO

Article history:
Received 5 January 2015
Received in revised form
10 April 2015
Accepted 14 April 2015
Available online 7 May 2015

Keywords:
Hydrogen storage
Mg–M–LiH alloys
Magnesium hydride
Mechanical alloying

ABSTRACT

$Mg_{96}M_2(LiH)_2$ (M = Y, Zn, Al, Ag), $Mg_{98}(LiH)_2$ and $Mg_{96}(LiH)_4$ powder alloys were produced by ball milling and deliberately air-exposed by 12 h in order to investigate their hydrogen storage properties. The addition of LiH at the level of 2 mol% had a beneficial effect on the kinetics of the hydriding and dehydriding processes at 300 and 350 °C compared to mechanically milled and air-exposed Mg powders. However, the additions of Al, Ag, Zn and Y had an opposite effect on the hydriding/dehydriding kinetics. The addition of Al provided a small advantage in the capacity of hydrogen storage among the tested materials. The effects of air-exposure were analyzed, it was demonstrated that among a set of Mg and Mg-alloys heavily oxidized the hydrogen storage is still viable.

Introduction

Magnesium is the archetypical material for hydrogen storage due to its high theoretical gravimetric hydrogen density of 7.6 wt.%. However, the main drawback of pure Mg/MgH_2 as a potential hydrogen storage material is the high temperature required for the dehydriding reaction, i.e., its high thermodynamic stability [1,2]. This drawback severely limits the possibility of use in mobile applications; nevertheless, stationary applications, high temperature fuel cells or heat storage are still feasible [3]. A second challenge is to obtain adequate hydriding and dehydriding kinetics. The beneficial influence of ball milling of Mg or MgH_2 is well known in this respect [4–6]; but still, the dehydriding kinetics are not considered sufficiently adequate. Theoretical and experimental results support the use of different transition metals in order to improve the kinetics, thermodynamics (or both

* *Corresponding author*. Universidad Nacional Autónoma de México, Instituto de Investigación en Materiales sede Morelia, Antigua Carretera a Pátzcuaro No. 8701, Col. Ex Hacienda de San José de la Huerta, C.P. 58190, Morelia, Michoacán, Mexico. Tel.: +52 5623 7300x80548.
E-mail addresses: karina_suarez@iim.unam.mx, karina.suarez.alcantara@gmail.com (K. Suárez-Alcántara).
http://dx.doi.org/10.1016/j.ijhydene.2015.04.083

simultaneously) of hydriding/dehydriding reactions [7–17]. In a previous work it has been observed that addition of small quantities of Zn, Al or Ag to Mg during ball milling improves the hydriding kinetics [18]. All together, these effects can be explained by the refinement of particle size and microstructure, increases in surface area, generation of crystalline defects on the surfaces and in the bulk, and the catalytic action of alloying metals or oxides, etc.

It is broad accepted that the handling of Mg and Mg-alloys must be performed under Ar-protective atmosphere as a way to avoid MgO formation. However, it must be considered that H_2 as fuel can be produced from different raw materials such as water, biomass, catalytic reforming of light hydrocarbons, etc.; where the high purity and homogeneity cannot always be guarantee. Also accidental air-exposure of materials during handling or operation is possible. Thus fabrication, processing and testing of our "traditional" materials under more purity-relaxed oxygen conditions must be done if extensive use of hydrogen storage materials is intended. We present a set of Mg-alloys; $Mg_{98}M_2(LiH)_2$ (M = Y, Zn, Al, Ag), exposed to air as hydrogen storage materials. The effects of the air-exposition on their hydrogen storage properties were analyzed. It was demonstrated that hydrogen storage is still viable at Mg-alloys heavily oxidized; this could lead to reduction of the costs of production, storage and handling in high-purity Argon protective atmosphere.

Materials and methods

Production of the powder alloys

$Mg_{96}M_2(LiH)_2$ (M = Al, Ag, Zn, Y), $Mg_{98}(LiH)_2$ and $Mg_{96}(LiH)_4$ powder alloys were prepared by mechanical milling. The corresponding molar quantities of elemental powders of Mg, Al, Ag, Zn, Y (99.8% purity, particle size < 45 μm) and LiH (99.9% purity, particle size < 3 μm) were used as received from Aldrich. The addition of LiH, in lieu of metallic Li, was considered a better approach to ensure the retention of Li in the final, as-milled powder mixtures. The mixtures were prepared in a Fritsch Pulverisette, model 6, milling device, at 350 rpm. The total effective milling time was 60 h in cycles of 1.5 h of milling and 0.5 h of pause. The ball-to-powder ratio was 11:1. The milling vial container (500 ml capacity) and the 50 balls of 1 cm diameter and 4 balls of 2 cm diameter were made of chromium steel. In total, 30 g of the powders plus 3 ml of methanol as milling control agent were charged in the container and sealed under Argon atmosphere.

After milling, the container was cooled to room temperature and the powders were gradually exposed to air for 12 h. Afterwards, these milled and passivated powders were stored in Ar-filled glass bottles. Subsequently, all handling for characterization was performed at open-air atmosphere. Pure Mg was given the same milling treatment, to be used as a reference and presented whenever needed below.

Hydriding and dehydriding reactions

Hydrogen storage properties were determined by means of a PCTM-6000 (Techno System Co., LTD) gravimetric equipment operating under chromatographically-pure hydrogen atmosphere. The equipment was carefully calibrated for pressure and temperature effects on the sample holder buoyancy. The alloys were subjected to hydriding and dehydriding activation cycles, before Pressure–Composition Isotherms (PCI) were determined. The activation cycles started with sample annealing at 350 °C under dynamic vacuum for 30 min. Then, the samples were subject to consecutive hydriding and dehydriding cycles at 350 °C. For the hydriding experiments, the hydrogen pressure was increased from 0.1 bar to 30 bar in steady pressure steps, the pressure increase ramp being performed in 25 min. The dehydriding process was carried out by reversing these conditions; the pressure decrease ramp was performed in 25 min. A single hydriding/dehydriding cycle took 6 h.

In the PCI determination, the hydrogen pressure increase/decrease steps in PCI measurements were 0.1 bar in the 0.1–1 bar interval and 1 bar in the 1–30 bar interval. The PCI measurement was performed in a total time of 16 h. After that, the temperature was fixed at 300 °C and a hydriding/dehydriding cycle was performed on the same sample. Finally, alloys were heated again at 350 °C and exposed to hydrogen at 30 bar for 3 h for further X-ray diffraction and scanning electron microscopy characterization of the hydrided powders.

Powder X-ray diffraction

X-ray diffraction (XRD) patterns were taken on a D-500 diffractometer (SIEMENS) using monochromatic CuKα1 (λ = 1.54056 Å) radiation. A scanning range from 15° to 80° was used with steps of 0.03° and 5 s per step. XRD patterns were taken without any atmosphere-protective layer, the samples being flat pressed in the sample holder. The MUAD software was used for XRD data processing [19].

Scanning electron microscope

The as-milled and hydrided alloys were observed in an XL/SFEG/SIRION SEM microscope (FEI Company) at 5 and 15 kV. A few milligrams of sample were attached to a carbon tape and transferred to the microscope chamber. All handing was performed in open air.

Results

XRD and SEM characterization of as-milled powders

XRD patterns of as milled powders are shown in Fig. 1. The diffraction peaks corresponding to magnesium, the major component, were clearly defined. Minor Fe contamination from the milling operation produced a small peak at about 44.5° in 2θ; Rietveld refinements (and EDS analysis, see below) account for less than 2 wt.% of Fe. The slight shifts in Mg peaks positions indicate a small distortion in cell lattice compared to the values found for as-milled pure Mg (Table 1, Mg ICSD-642651). These distortions can be attributed to alloying effects. The addition of LiH produced minor distortions in the Mg lattice in $Mg_{98}(LiH)_2$ and $Mg_{96}(LiH)_4$, as indicated in Table 1. A noticeable lattice contraction was observed in $Mg_{96}Al_2(LiH)_2$,

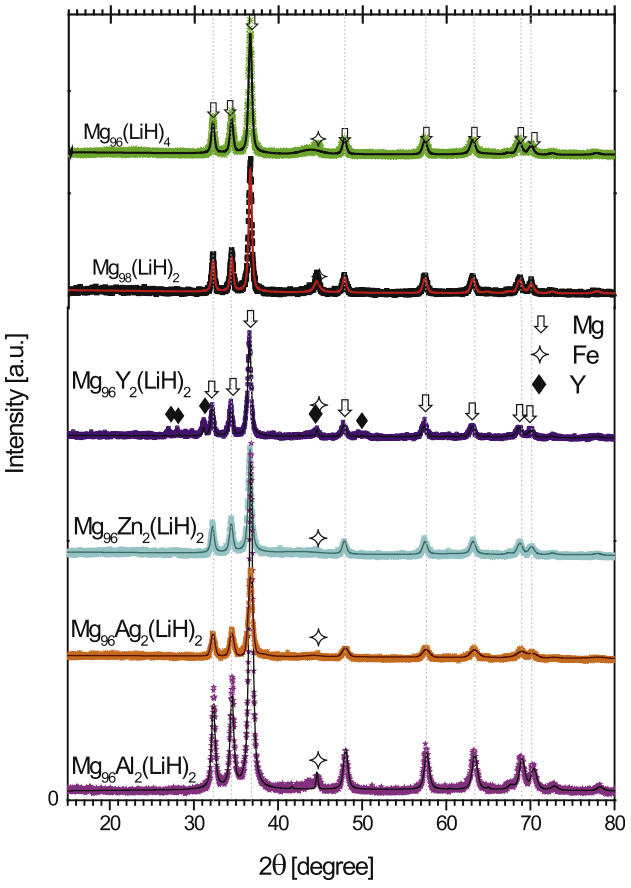

Fig. 1 – XRD patterns of as-milled and air-exposed powders. Dots: experimental patterns. Line:refined patterns.

probably due to the smaller atomic size and larger valency of Al compared to Mg. The $Mg_{96}Al_2(LiH)_2$ mixture presented the larger contraction in the Mg lattice among the tested materials. Lattice contraction was also observed in $Mg_{96}Ag_2(LiH)_2$ and $Mg_{96}Zn_2(LiH)_2$, but to a lesser extent compared to $Mg_{96}Al_2(LiH)_2$. In the $Mg_{96}Y_2(LiH)_2$ powder mixture, the unit cell contraction was only detected in the "c" axis. Table 1 collects the refined Mg cell lattice parameters calculated for our materials. Goodness of fit figures are also included in Table 1.

Mg crystallite sizes estimated by means of the Rietveld refinement of the X-ray patterns of the as-milled materials are also collected in Table 1. The data reveal that ball milled $Mg_{96}Al_2(LiH)_2$, $Mg_{96}Zn_2(LiH)_2$ and $Mg_{96}Y_2(LiH)_2$ had crystallite sizes of about 30 nm; i.e., a slight reduction from the ~35–40 nm of pure Mg, $Mg_{98}(LiH)_2$ and $Mg_{96}(LiH)_4$ powders. The calculated value for $Mg_{96}Ag_2(LiH)_2$ was significantly different from all other samples, presenting a crystallite size of about 100 nm.

Despite the affinity of Mg for oxygen and the exposure of the as-milled powders to air at the time of removing them from the milling vial, no clear indication for the formation of crystalline MgO is found in the XRD patterns of Fig. 1. We will come back to this point in the Discussion Section Effect of MgO on hydrogen storage properties.

The as-milled powders were extensively agglomerated. The agglomerate size shows a wide dispersion, as illustrated on the SEM micrograph displayed in Fig. 2 (see supplementary file for more SEM pictures of all materials). Most agglomerates possess sizes in the interval of 1–10 μm. Nevertheless, *individual* particles can be observed with sizes clearly below 1 μm. In many instances, the SEM images provide evidence for the occurrence of cold-welding among small particles during milling, as the mechanism of formation of the agglomerates.

Hydriding and dehydriding experiments

Fig. 3 presents the $Mg_{98}(LiH)_2$ cycling behavior at 350 °C as representative of all our tested materials. The hydrogenation at the first cycle was slow and incomplete within the presented time frame. As cycling proceeded the hydrogen uptake and hydriding/dehydriding kinetics were improved. Fig. 4a presents the first 60 min of the absorption part of the third hydriding/dehydriding treatment applied to all the mechanically milled powders at 350 °C. The pressure increase up to 30 bar is also plotted (grey line). Results for as-milled Mg powders are included for comparison. Mg absorbed about 5.0 wt.% H_2 in 60 min and 5.1 wt.% at the end of experiment; i.e. the smaller value of hydrogen uptake of all the studied alloys. The $Mg_{98}(LiH)_2$ and $Mg_{96}(LiH)_4$ mixtures present the fastest kinetics, with a maximum hydrogen uptake of about 5.5 wt. %. In both materials the hydriding reaction is completed in 24 min. The $Mg_{96}Al_2(LiH)_2$ mixture also showed good hydriding kinetics and good hydrogen uptake. This mixture completed the hydrogen uptake in 36 min; it absorbed 6.2 wt.% H_2. Among the ternary alloys, the $Mg_{96}Ag_2(LiH)_2$ mixture presented the slowest hydriding kinetics, even slower than Mg. After 63 min, time to complete the hydrogen uptake, $Mg_{96}Ag_2(LiH)_2$ stored 5.8 wt.% of H_2. $Mg_{96}Zn_2(LiH)_2$ presented

Table 1 – Unit Cell parameters and crystallite size of as-milled materials estimated from XRD refinement.

As-milled material	Mg unit cell [Å] ICSD-642651 a = b = 3.2094 Å c = 5.2108 Å	Mg crystallite size [nm]	Goodness of fit: GofF = R_{wp}/R_{exp}
Mg	a = b = 3.2096 ± 2 × 10^{-4} Å c = 5.2129 ± 5 × 10^{-4} Å	36.4 ± 3.9	1.39
$Mg_{98}(LiH)_2$	a = b = 3.2114 ± 4 × 10^{-4} Å c = 5.2126 ± 8 × 10^{-4} Å	37.4 ± 1.0	2.28
$Mg_{96}(LiH)_4$	a = b = 3.2090 ± 2 × 10^{-4} Å c = 5.2084 ± 6 × 10^{-4} Å	40.2 ± 0.6	2.94
$Mg_{96}Al_2(LiH)_2$	a = b = 3.1949 ± 2 × 10^{-4} Å c = 5.1904 ± 5 × 10^{-4} Å	27.8 ± 0.3	1.32
$Mg_{96}Ag_2(LiH)_2$	a = b = 3.2002 ± 5 × 10^{-4} Å c = 5.1927 ± 9 × 10^{-4} Å	97.7 ± 14.3	1.05
$Mg_{96}Zn_2(LiH)_2$	a = b = 3.2080 ± 5 × 10^{-4} Å c = 5.2080 ± 9 × 10^{-4} Å	30.4 ± 0.3	0.90
$Mg_{96}Y_2(LiH)_2$	a = b = 3.2097 ± 5 × 10^{-4} Å c = 5.2093 ± 9 × 10^{-4} Å	33.3 ± 0.8	1.11

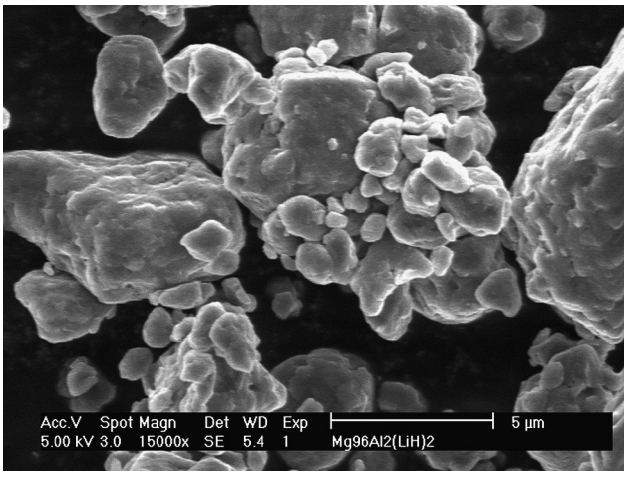

Fig. 2 – SEM micrograph of as-milled and air-exposed $Mg_{96}Al_2(LiH)_2$.

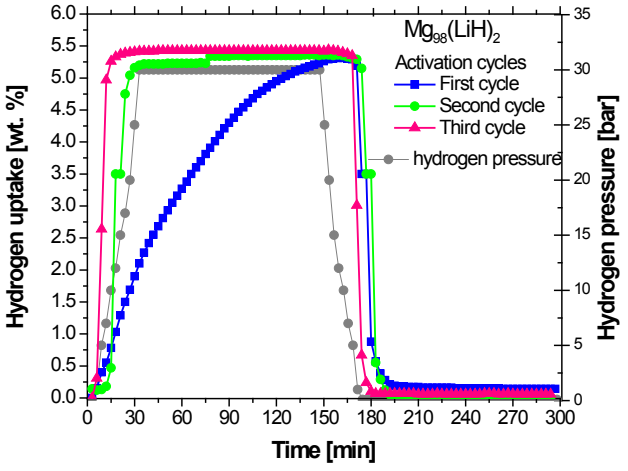

Fig. 3 – $Mg_{98}(LiH)_2$ cycling behavior at 350 °C.

kinetics similar to Mg; after 45 min at the hydriding conditions it absorbed 5.2 wt.% as maximum amount of H_2. $Mg_{96}Y_2(LiH)_2$ powders presented good kinetics, the reaction is essentially completed in 27 min (5.3 wt.% H_2) and the maximum amount of 5.6 wt.% at the end of experiment. Table 2 condenses the hydriding characteristics of all the materials tested in the present work. These values are reported at the time of reaching 80% of the maximum hydrogen uptake ($\alpha = 0.8$, where α is the transformed fraction, i.e. the ratio between the current hydrogen uptake and the final hydrogen uptake) and at the end of experiment (140 min).

The corresponding hydriding processes at 300 °C and 30 bar are presented in Fig. 4b (first 60 min). At this temperature, $Mg_{98}(LiH)_2$ and $Mg_{96}(LiH)_4$ had the fastest kinetics, completing the reaction in 30 min. The $Mg_{96}Al_2(LiH)_2$ mixture showed again the highest hydrogen uptake (6.1 wt.%), completed in 39 min. $Mg_{98}Ag_2(LiH)_2$ and $Mg_{96}Zn_2(LiH)_2$ showed the slowest hydriding kinetics, even slower than Mg. The hydriding reactions in these materials were completed in 105 and 129 min, respectively. $Mg_{96}Y_2(LiH)_2$ and Mg presented similar slower kinetics and hydrogen uptake (about 57 min to saturate; 5.3 wt.% and 5.0 wt.%, respectively). Table 2 summarizes the features of the hydriding processes displayed in Fig. 4b.

Fig. 5a presents the results of the dehydriding experiments at 350 °C. It should be noted that the thermogravimetric equipment used in our experiments was programmed with steps of small pressure changes; large changes in pressure could lead to disturbances. Therefore, the initial time for this stage was taken when the pressure was still 30 bar (grey line); actually, the dehydriding reaction started at about 5 bar for $Mg_{98}(LiH)_2$ and $Mg_{96}(LiH)_4$ (18 min) and at about 0.1 bar for the ternary alloys (24 min). The times for completion of the dehydriding stage at 350 °C are collected in Table 3. The values are reported as "effective" values, by taking time zero as the minute 18 (5 bar) for the binary materials and 24 (0.1 bar) for the ternary materials, i.e., the actual pressures at which the dehydriding stage started. $Mg_{98}(LiH)_2$ and $Mg_{96}(LiH)_4$ presented a clear improvement on dehydriding kinetics

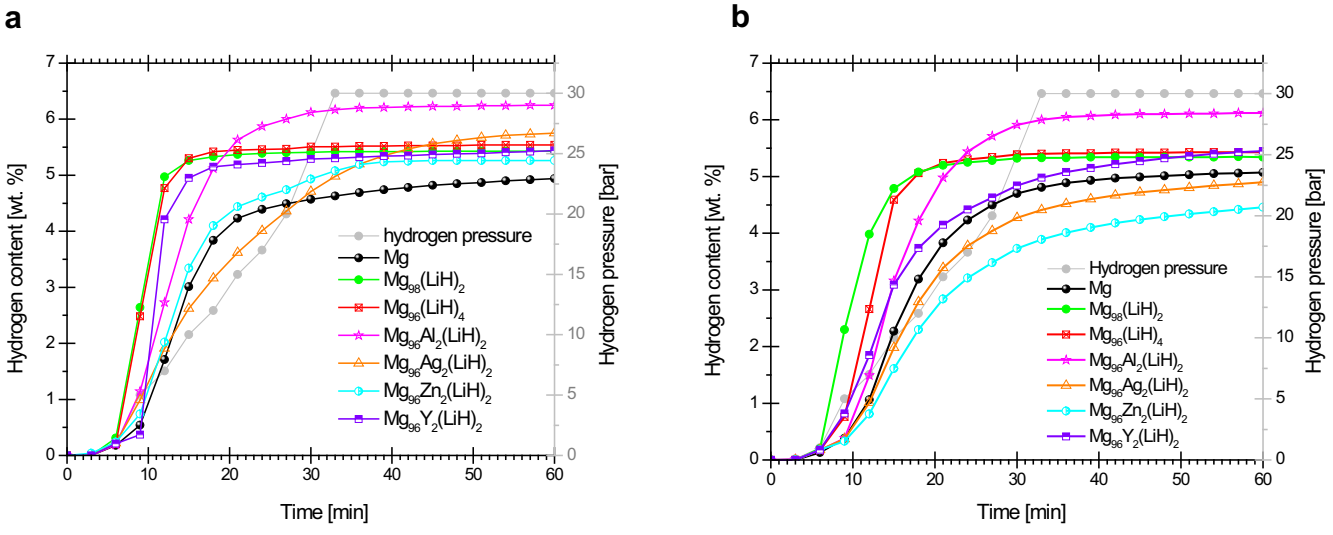

Fig. 4 – a. Hydriding stage at 350 °C in the mechanically alloyed powders and pure Mg. b. Hydriding stage at 300 °C in the mechanically alloyed powders and pure Mg.

Table 2 – Summary of hydriding characteristics at 350 and 300 °C. In parenthesis, values from the PCI curves.

Material	350 °C/30 bar		300 °C/30 bar	
	t_{sat} [min][a]	Hydrogen content [wt.%] (theoretical; max[b]; PCI)	t_{sat} [min][a]	Hydrogen content [wt.%] (max[b]; PCI)
$Mg_{98}(LiH)_2$	11	7.55; 5.4; 5.3	13	5.3; 5.3
$Mg_{96}(LiH)_4$	12	7.51; 5.6; 5.5	15	5.4; 5.3
$Mg_{96}Al_2(LiH)_2$	18	7.40; 6.2; 6.0	21	6.1; 6.0
$Mg_{96}Ag_2(LiH)_2$	30	6.96; 5.8; 5.5	28	5.2; 5.2
$Mg_{96}Zn_2(LiH)_2$	19	7.18; 5.3; 5.0	36	5.0; 4.9
$Mg_{96}Y_2(LiH)_2$	13	7.06; 5.6; 5.8	24	5.6; 4.8
Mg	20	7.60; 5.1; 4.9	23	5.1; 5.1

[a] $\alpha = 0.8$ of reaction yield.
[b] at 140 min.

compared with Mg. The reaction is completed in a few minutes for the binary alloys. With some minor differences, the dehydriding kinetics of the Al- and Ag-containing ternary alloys followed the same behavior than Mg. Some hydrogen content (<0.4 wt.%) seem to remain in some of the alloys according to the curves in Fig. 5a, but this amount may be within the accuracy (zero level) of the testing procedure. The Zn- and Y- containing ternary alloys showed a slight kinetic improvement compared to Mg.

Finally, the kinetics of dehydriding at 300 °C are shown in Fig. 5b. The same correction for an "effective" time is considered in this case for the actual pressures at which the dehydriding reactions began. Here again, the process occurs faster in the $Mg_{98}(LiH)_2$ and $Mg_{96}(LiH)_4$ powders (36 and 60 min to completion, respectively; effective time), followed by the $Mg_{96}Y_2(LiH)_2$ powders (~ 87 min). The remaining alloys did not complete the dehydriding stage at this temperature within the 2.5 h that the experiments were run. However, it can be seen from Fig. 5a and b that the dehydriding kinetics were rather similar in the $Mg_{96}Zn_2(LiH)_2$ and $Mg_{96}Ag_2(LiH)_2$ powders. In

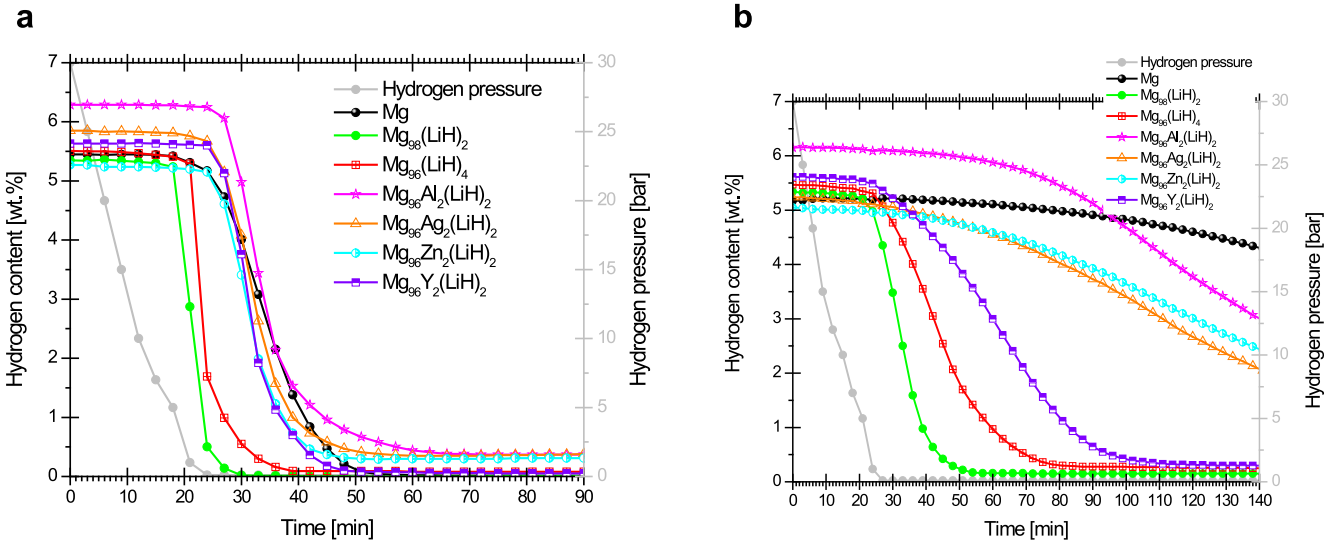

Fig. 5 – a. De-hydriding stage at 350 °C in the mechanically alloyed powders and pure Mg. b. De-hydriding stage at 300 °C in the mechanically alloyed powders and pure Mg.

Table 3 – Summary of dehydriding characteristics at 350 and 300 °C.

Material	350 °C/0.1 bar		300 °C/0.1 bar	
	t_{end} [min][a,b]	H Remaining after 140 min [wt.%]	t_{end} [min][a,b]	H Remaining after 140 min [wt.%]
$Mg_{98}(LiH)_2$	5	0	20	0.2
$Mg_{96}(LiH)_4$	9	0	40	0.3
$Mg_{96}Al_2(LiH)_2$	18	0.4	116	3.0
$Mg_{96}Ag_2(LiH)_2$	16	0.4	>116	2.0
$Mg_{96}Zn_2(LiH)_2$	13	0.3	>116	2.4
$Mg_{96}Y_2(LiH)_2$	12	0	57	0.3
Mg	17	0	>116	4.3

[a] $\alpha = 0.8$ of reaction yield.
[b] Effective time (registered time minus the beginning time of reaction); 18 min for $Mg_{98}(LiH)_2$ and $Mg_{96}(LiH)_4$; and 24 min for Mg and ternary alloys.

turn, the $Mg_{96}Al_2(LiH)_2$ and Mg samples exhibited the slowest kinetic behavior. Table 3 summarizes the features of the dehydriding processes displayed in Figs. 4b and 5b. Hydriding/dehydriding and PCI details of $Mg_{98}(LiH)_2$ and $Mg_{98}(LiH)_2$ are available in the supplementary file.

Due to time-constraining conditions, the PCI curves where not taken strictly at equilibrium conditions; hereafter, these curves are called quasi-PCI curves. The quasi-PCI curves determined at 350 °C are presented in Fig. 6. The upper frame of Fig. 6 displays the quasi-PCI curves of Mg, $Mg_{98}(LiH)_2$ and $Mg_{96}(LiH)_4$. The lower frame presents the ternary alloys quasi-PCI curves. The hydriding curves presented plateaus at similar pressures (~ 8 bar) for all the alloyed powders, whereas for Mg the plateau was not well defined; however, the middle point at the semi-plateau is located about 16 bar. The dehydriding quasi-PCI curves at 350° seem to be established under conditions close to equilibrium; in this case, the plateau pressures vary randomly with alloy composition in the range from approximately 2 bar–4 bar, with the exception of Mg, for which the plateau pressure is about 0.7 bar. From Fig. 6 it can be observed that alloying with Li induced a reduction in the hydriding/dehydriding hysteresis compared with Mg. In turn, Al, Ag Zn and Y alloying did not introduce further changes. The reduction of hydriding quasi-plateau pressure and the increase of the dehydriding quasi-plateau pressure upon alloying is a change in the correct direction to improve the hydriding/dehydriding properties of these air-exposed materials.

XRD and SEM characterization of hydrided powders

Fig. 7 presents the XRD patterns from powder mixtures which underwent a final hydriding treatment at 350 °C and 30 bar after the determination of the corresponding quasi-PCI curves. As observed in a number of previous studies [20,21], the XRD patterns presented a broad peak at the 2θ position expected for the main reflection from MgO. The Rietveld-estimated crystal size of MgO is about 4–7 nm. Table 4 presents the composition estimated by Rietveld refinement. The main components are MgH_2 and MgO; the remaining components are elemental Mg, and Fe. Table 4 also collects the MgH_2 unit cell parameters and crystallite size obtained from the Rietveld refinement of the XRD data. No correlation of the cell parameters with the alloy components was found. Still, the samples $Mg_{96}Al_2(LiH)_2$ and, unexpectedly, $Mg_{96}Zn_2(LiH)_2$ retain the smallest MgH_2 unit cell size. The MgH_2 phase presented a sensible increase of the crystallite size compared with the initial Mg crystallite size in all samples. The $Mg_{98}(LiH)_2$ and $Mg_{96}(LiH)_4$ samples have the smallest crystallite sizes. This corresponds also with the quickest dehydriding kinetics. Goodness of fit figures are also included in Table 4. The longer than expected figures at hydrided $Mg_{96}M_2(LiH)_2$ (M = Al, Ag, Zn, Y) materials come from the difficulty on noise background modeling.

A representative SEM picture of the hydrided materials is presented in Fig. 8. More images are available as supporting info. The surface of the hydrided materials presented

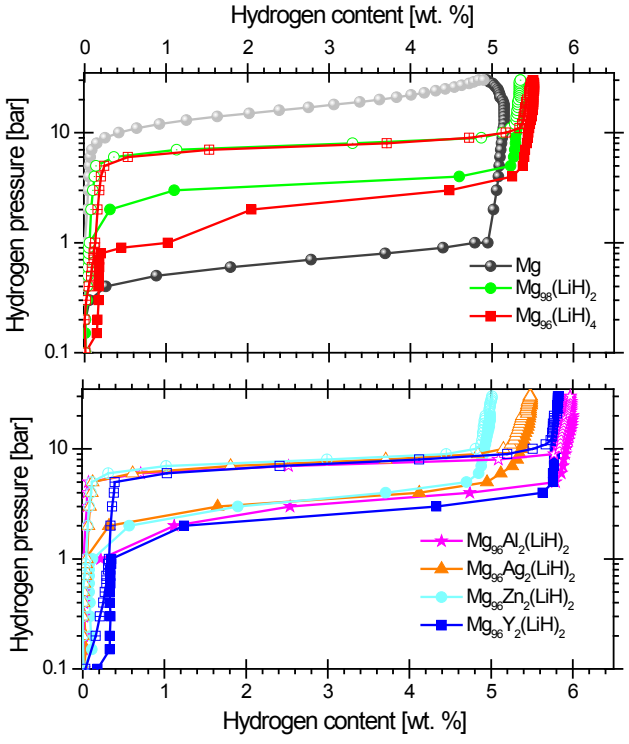

Fig. 6 – PCI curves determined at 350 °C. Open dots: hydriding. Closed dots: dehydriding.

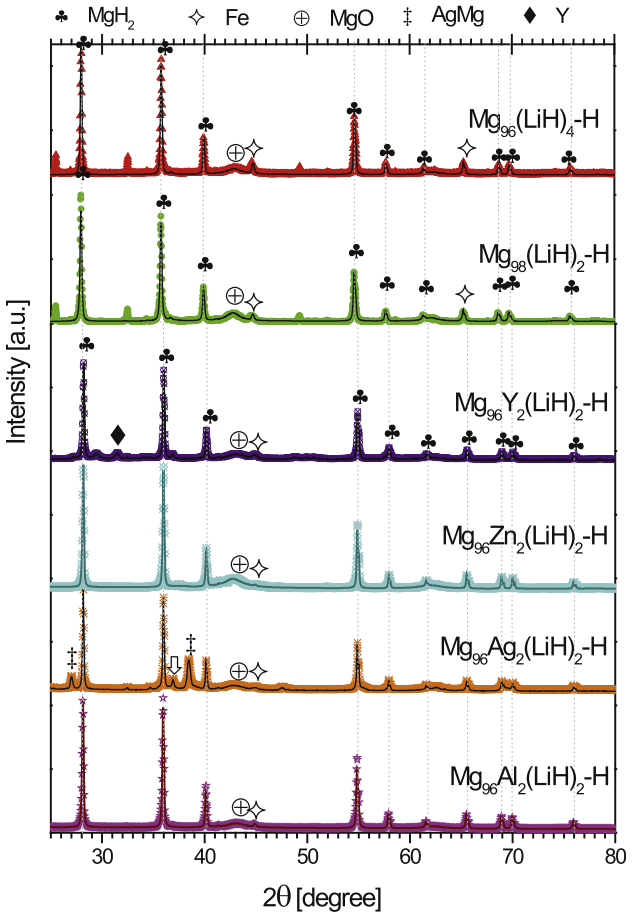

Fig. 7 – XRD patterns of hydrided powders at 350 °C and 30 bar hydrogen pressure. Dots:experimental patterns. Line: refined patterns.

Table 4 – Unit cell parameters and crystallite size of hydrided materials at 350 °C and 30 bar H_2. Data estimated from XRD refinement.

Hydrided material	Composition [wt.%]	MgH_2 unit cell [Å] ICSD-161962 a = b = 4.5140 c = 2.9920	MgH_2 crystallite size [nm]	MgO crystallite size [nm]	Goodness of fit: GofF = R_{wp}/R_{exp}
Mg	Mg: 21.0 ± 1.0 MgH_2: 60.1 ± 1.2 MgO: 18.9 ± 0.7	a = b = 4.5215 ± 4.2 × 10^{-4} c = 3.0233 ± 3.5 × 10^{-4}	57.3 ± 6.2	5.6 ± 0.2	1.15
$Mg_{98}(LiH)_2$	Mg: 0.8 ± 0.1 MgH_2: 61.4 ± 3.0 MgO: 36.7 ± 1.0 Fe: 1.0 ± 0.1	a = b = 4.5223 ± 4.6 × 10^{-4} c = 3.0244 ± 3.4 × 10^{-4}	131.7 ± 4.9	7.1 ± 0.2	2.04
$Mg_{96}(LiH)_4$	Mg: 0.8 ± 0.1 MgH_2: 67.9 ± 1.0 MgO: 29.2 ± 0.8 Fe: 2.0 ± 0.1	a = b = 4.5217 ± 2.9 × 10^{-4} c = 3.0241 ± 2.4 × 10^{-4}	129.3 ± 4.3	5.9 ± 0.2	2.14
$Mg_{96}Al_2(LiH)_2$	MgH_2: 72.9 ± 1.0 MgO: 26.4 ± 0.5 Fe: 0.6 ± 0.1	a = b = 4.5182 ± 6.8 × 10^{-4} c = 3.0219 ± 4.8 × 10^{-4}	191.4 ± 17.9	5.1 ± 0.1	7.96
$Mg_{96}Ag_2(LiH)_2$	Mg: 5.0 ± 0.3 MgH_2: 54.9 ± 1.0 MgO: 34.8 ± 1.3 MgAg: 5.1 ± 0.1 Fe: 1.0 ± 0.1	a = b = 4.5221 ± 3.1 × 10^{-4} c = 3.0241 ± 2.3 × 10^{-4}	217.9 ± 12.1	4.6 ± 0.2	8.50
$Mg_{96}Zn_2(LiH)_2$	MgH_2: 53.0 ± 1.0 MgO: 45.2 ± 0.9 Zn: 1.6 ± 0.1 Fe: 0.2 ± 0.05	a = b = 4.5178 ± 3.6 × 10^{-4} c = 3.0217 ± 2.5 × 10^{-4}	258.4 ± 16.9	4.1 ± 0.1	8.56
$Mg_{96}Y_2(LiH)_2$	MgH_2: 67.3 ± 1.0 MgO: 28.8 ± 0.9 Y: 1.7 ± 0.8 Fe: 2.1 ± 0.1	a = b = 4.5196 ± 2.9 × 10^{-4} c = 3.0228 ± 2.1 × 10^{-4}	196.8 ± 8.8	6.8 ± 0.3	8.49

protuberances. This has been related with the nucleation and growing of MgH_2 over Mg particles [22].

Discussion

LiH effect on hydrogen storage properties

The results presented in this paper have indicated a significant accelerating effect of the kinetics of hydriding/dehydriding reactions in oxide-covered Mg-base alloys by the addition of a small amount of LiH. Interestingly and novelty, the addition of 2 mol% LiH had a significantly higher accelerating effect than a larger addition of 4 mol%. In terms of the times to reach uptake saturation and complete dehydriding (Tables 2 and 3); the kinetics in the $Mg_{98}(LiH)_2$ mixture improved by a factor of 2 in hydriding, and at least by 3 in dehydriding processes in comparison to as-milled Mg. Smith et al. [23] in a recent theoretical study on the substitution of Li^+ for Mg^{2+} in MgH_2 indicates that Li doping may enhance the hydrogen diffusion but only to a limited extent determined by an optimal dopant concentration. Liang et al. [24] and Huot et al. [25] previously reported some hydrogen storage properties of Mg–Li alloyed powders produced by mechanical alloying. In the work of Liang et al., the amount of Li was 10 at %, but vanadium and graphite were also added in the amounts of 2.5 at% and 2 wt.%, respectively [24]. Despite the expected catalytic activity of vanadium in this material, the reported kinetics of hydriding/dehydriding processes at 350 °C are comparable to what is shown for our Mg–LiH alloys in Figs. 4a and 5a. On the other hand, the final materials prepared by Huot et al. [25] by lixiviation of Li from a mechanically alloyed Mg- 28 at% Li powder mixture, probably contained a small amount of Li (no final chemical analysis was given by the authors). In this case also the kinetics of hydriding/dehydriding are close to those found in our work, at the same temperature of 350 °C. These authors suggested that the improved kinetics in their materials (as compared to Mg) was mainly the result of a much larger specific surface area in the lixiviated products. Taken together, the work of Liang et al.

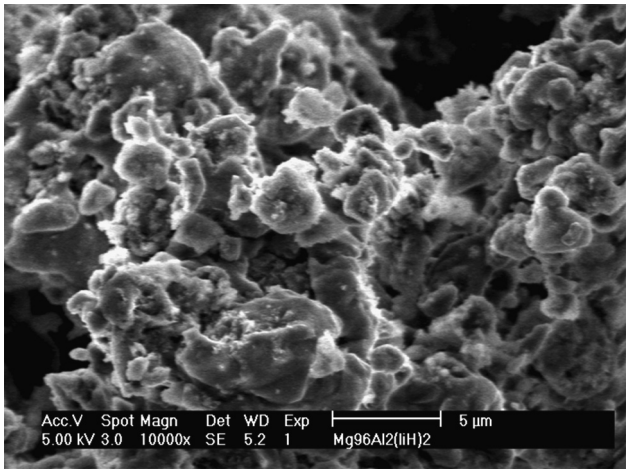

Fig. 8 – SEM micrograph of hydrided $Mg_{96}Al_2(LiH)_2$ at 350 °C and 30 bar hydrogen pressure.

and Huot et al. seem to be consistent with the results of our own in that a small addition of Li induces considerably beneficial kinetics effects in the hydrogen storage properties of Mg powders.

The mechanisms by which Li influences the hydrogen storage characteristics of Mg powders may be complex and are open to debate. In a recent paper, Palacios et al. [26] had shown that a mixed hydride of the composition $Mg_{15}LiH_{32}$ has a lower thermodynamic stability than pure MgH_2 ($\Delta H_f = -58.3$ kJ mol^{-1} and $\Delta H_f = -71.7$ kJ mol^{-1} respectively); this, by itself, it is usually taken as a good indication of lower decomposition temperatures for the hydride phase [27], or conversely, faster reaction kinetics at a given temperature. A destabilizing effect had been observed in other Li-containing hydrogen storage materials such as $LiBH_4/MgH_2$ [28]. Nonetheless, the full explanation of the hydriding/dehydriding kinetics of our Mg–LiH powders is not solely based on the thermodynamic stability of the different hydrides, but also in structural factors.

Effect of M (M = al, Ag, Zn and Y) additions on hydrogen storage properties

The findings presented here shed light on the effect of the addition of small quantities of metals to Mg over the hydrogen storage properties. It is clear from the kinetics and PCI data (Figs. 4–6) that the addition of Ag, Zn and Y in the ternary powder mixtures did not represent any benefit to the hydrogen storage properties over those obtained by the addition of LiH alone. On the contrary, in these cases the ternary addition resulted in unfavorable properties compared to those shown by as-milled Mg, our reference material. Only the addition of Al seems to have improved the hydrogen uptake, but not the hydriding/dehydriding kinetics. Surprisingly, despite the large volume of literature dedicated to the hydrogen storage properties of Mg-based alloys, we have not found reports involving dilute, binary alloys of Al, Ag, Zn or Y in magnesium in which a consistent comparison of their hydriding/dehydriding properties with those of Mg was accomplished. A semi-quantitative comparison of mechanically milled Mg powders with mechanically alloyed Mg-M mixtures (M = Al, Ag, Zn and Y), having a nominal content of 2 at% M, was presented recently by Palacios et al. [18]. According to their results, the additions of these elements had the effect of reducing the formation of MgH_2 in basically all the alloyed powders and hydriding conditions.

Effect of MgO on hydrogen storage properties

An amorphous layer or islands of MgO could be formed during the air-exposure step after ball milling, which would become crystalline when being subjected to higher temperatures, as suggested by the XRD of as-milled and hydrided materials. Shih et al. [29] proposed the mechamisn of MgO formation over Mg as the following successive steps: oxygen chemisorption on the magnesium surface, formation and coalescence of oxide islands and oxide thickening. It was believed for a long time that the formation of oxide layers prevented at all further hydrogen uptake in Mg materials [30]. However, it was recently reported that the addition up to 10 wt.% of MgO to MgH_2 can reduce the dehydriding temperature to 262 °C [31]. Barkhordarian et al. demonstrated the potential use of metal oxides as suitable catalyst for hydrogen storage purposes [32]. In both reports, the metal oxides were milled together with the MgH_2. Borgschulte et al. [33] demonstrated that a surface layer of MgO is able to recombine atomic hydrogen. Friedrichs et al. performed a hydrogen desorption kinetics study of air-exposed Mg catalyzed with 2 mol% of Nb_2O_5 [34]. In that study; in the sample exposed to air for 24 h, the hydrided Mg was able to desorb about 3 wt.% hydrogen at 300 °C and 0.001 bar in 30 min. The 1 h air-exposed sample was able to desorb about 4 wt. % under the same conditions. As a novelty, the present work demonstrates that 5.0 to 6.2 wt.% hydrogen storage is still feasible after deliberate air-exposure for 12 h our Mg alloys. Meanwhile, the amount of MgO formed is apparently between 18.9 and 45.2 wt%. Similar MgO weight fractions had been frequently determined in a number of studies [18,35]. Let us remark that this drop in storage capacity is a frequent observation in the literature on Mg-based alloys [36–39]. A second common observation in such cases is the existence of a considerable amount of "disordered" magnesium oxide [37,38,40], evidently as a consequence of the high affinity of magnesium for oxygen and the large amount of "fresh" (reactive) surface area found in powders right after their production and/or after being subjected to a dehydriding treatment.

Two phenomenon have been proposed for explaining the observed dehydriding reactions at MgO covered MgH_2 [33]: (1) that the inactive MgO forms nano or micro-cracks, channels or pathways [29,34], exposing fresh and active Mg/MgH_2 surfaces; and (2) that the MgO formed on top of MgH_2 is indeed active by the formation of oxygen vacancies during hydrogen exposure and heating [34]. The SEM images (at the micrometer observation size range) do not reveal cracks or fissures on the surface of the powder particles, but the agglomerates look smaller in size. The cycling behavior presented in Fig. 3 (common to all our samples), indicates the dificulty of performing the first hydriding reaction. This is consistent with the existence of an obstructive layer. Shih et al. [29] also proposed that the different thermal expansion coefficients of Mg and MgO could lead to cracks in the oxide film. This can explain in part the improvement in the hydriding/dehydriding kinetics after cycling.

Conclusions

Mg, $Mg_{98}(LiH)_2$, $Mg_{96}(LiH)_4$ and $Mg_{96}M_2(LiH)_2$ (M = Al, Ag, Zn and Y) alloys were produced by mechanical alloying and deliberately air-exposed after milling. Despite the formation of MgO, this alloy production technique is still suitable for hydrogen storage materials and has the potential to reduce the cost of using a high purity protective atmosphere during alloy fabrication and handling. A maximum hydrogen storage of 6.2 wt.% was obtained at $Mg_{96}Al_2(LiH)_2$; 5.1 wt.% was the minimum hydrogen storage capacity obtained at Mg (350 °C/30 bar). The addition of LiH to Mg improved the hydrogen sorption/desorption kinetics; an addition of LiH at the level of 2 mol % had the best effect on the kinetics of the hydriding and dehydriding processes at 300 and 350 °C. Further addition of Al, Ag, Zn or Y to

$Mg_{96}(LiH)_4$ does not improve the kinetics of hydriding/dehydriding. We attribute the changes in hydriding/dehydriding kinetics of our Mg–LiH powders to structural factors.

Acknowledgements

KSA and JGCM thank CINVESTAV for technical support. KSA thanks DGECI-UNAM for a mobility grant.

Appendix A. Supplementary data

Supplementary data related to this article can be found at http://dx.doi.org/10.1016/j.ijhydene.2015.04.083.

REFERENCES

[1] Bowman Jr RC, Fultz B. Metallic hydrides I: hydrogen storage and other gas-phase applications. MRS Bull 2002;27:688–93.
[2] Schlapbach L, Züttel A. Hydrogen-storage materials for mobile applications. Nature 2001;414:353–8.
[3] Felderhoff M, Bogdanović B. High temperature metal hydrides as heat storage materials for solar and related applications. Int J Mol Sci 2009;10:325–44.
[4] Huot J, Liang G, Schulz R. Mechanically alloyed metal hydride systems. Appl Phys A 2001;72:187–95.
[5] Buschow KHJ, Bouten PCP, Miedema AR. Hydrides formed from intermetallic compounds of two transition metals: a special class of ternary alloys. Rep Prog Phys 1982;45:937–1039.
[6] Hanada N, Ichikawa T, Orimo SI, Fujii H. Correlation between hydrogen storage properties and structural characteristics in mechanically milled magnesium hydride MgH_2. J Alloys Compd 2004;366:269–73.
[7] Er S, Tiwari D, Wijs GA, Brocks G. Tunable hydrogen storage in magnesium–transition metal compounds: first-principles calculations. Phys Rev B 2009;79:024105.
[8] Luo FP, Wang H, Ouyang LZ, Zeng MQ, Liua JW, Zhua M. Enhanced reversible hydrogen storage properties of a Mg–In–Y ternary solid solution. Int J Hydrogen Energy 2013;38:10912–8.
[9] Shao H, Felderhoff M, Schuth F, Weidenthaler C. Nanostructured Ti-catalyzed MgH_2 for hydrogen storage. Nanotechnology 2011;22:235401–7.
[10] Baum L, Meyer M, Mendoza-Zélis L. Hydrogen storage properties of the Mg/Fe system. Phys B Condens Matter 2007;389:189–92.
[11] Song Y, Guo ZX, Yang R. Influence of selected alloying elements on the stability of magnesium dihydride for hydrogen storage applications: a first-principles investigation. Phys Rev B 2004;69:094205–11.
[12] Miwa K, Fukumo A. A first-principles study on 3d transition-metal dihydrides. Phys Rev B 2002;65:155114–7.
[13] Nakatsuka K, Yoshino M, Yukawa H, Morinaga M. Roles of the hydride forming and non-forming elements in hydrogen storage alloys. J Alloys Compd 1999;293–295:222–6.
[14] Yukawa H, Matsumura T, Morinaga M. Chemical bond state and hydride stability of hydrogen storage alloys. J Alloys Compd 1999;293–295:227–30.
[15] Smithson H, Marianetti CA, Morgan D, Van der Ven A, Predith A, Ceder G. First-principles study of the stability and electronic structure of metal hydrides. Phys Rev B 2002;66:144107–10.
[16] Grochala W, Edwards PP. Chemical tuning of the thermal decomposition temperature of inorganic hydrides: computational aspects. J Alloys Compd 2005;404–406:31–4.
[17] Hanada N, Ichikawa T, Hino S, Fujii H. Remarkable improvement of hydrogen sorption kinetics in magnesium catalyzed with Nb_2O_5. J Alloys Compd 2006;420:46–9.
[18] Palacios-Lazcano AF, Luna-Sánchez JL, Cruz-Gandarilla F, Cabañas-Moreno JG. Hydrogen storage in nanostructures Mg-base alloys. J Nano Res 2009;5:213–21.
[19] Lutterotti L. Maud: a Rietveld analysis program designed for the internet and experiment integration. Acta Cryst 2000;A56 (Supplement) s54.
[20] Huot J, Liang G, Boily S, Van Neste A, Schulz R. Structural study and hydrogen sorption kinetics of ball-milled magnesium hydride. J Alloys Compd 1999;293–295:495–500.
[21] Varin RA, Lia S, Calka A. Environmental degradation by hydrolysis of nanostructured-MgH_2 hydride synthesized by controlled reactive mechanical milling (CRMM) of Mg. J Alloys Compd 2004;376:222–31.
[22] Mooij L, Dam B. Nucleation and growth mechanisms of nanomagnesium hydride from the hydrogen sorption kinetics. Phys Chem Chem Phys 2013;15:11501–10.
[23] Smith KC, Fisher TS, Waghmare UV, Grau-Crespo R. Dopant-vacancy binding effects in Li-doped magnesium hydride. Phys Rev B 2010;82. 134109–9.
[24] Liang G. Synthesis and hydrogen strorage properties of Mg-based alloys. J Alloys Compd 2004;370:123–8.
[25] Huot J, Bouaricha S, Boily S, Dodelet JP, Guay D, Schulz R. Increase of specific surface area of metal hydrides by lixiviation. J Alloys Compd 1998;266:307–10.
[26] Palacios-Lazcano AF, Yukawa H, Morinaga M, Cabañas-Moreno JG. Stability of mixed magnesium hydrides (Mg–M) H_2 (M = Al, Ag, Ga, Li, Sc, Y, Zn) estimated by density functional theory. Submitted to Trans JIM. 2014.
[27] Grochala W, Edwards P. Thermal decomposition of the non-intersitial hydrides for the storage and production of hydrogen. Chem Rev 2004;104:1283–315.
[28] Price TEC, Grant DM, Weston D, Hansen T, Arnbjerg LM, Ravnsbæk DB, et al. The effect of H_2 partial pressure on the reaction progression and reversibility of lithium-containing multicomponent destabilized hydrogen storage systems. J Am Chem Soc 2011;133:13534–8.
[29] Shih TS, Liu YB, Wei PS. Oxide films on magnesium alloys. Mater Chem Phys 2007;104:497–504.
[30] Ostenfeld CW, Johansson M, Chorkendorff I. Hydrogenation properties of catalyzed and non-catalyzed magnesium films. Surf Sci 2007;601:1862–9.
[31] Ares-Fernández JR, Aguey-Zinsou KF. Superior MgH_2 kinetics with MgO addition: a tribological effect. Catalysts 2012;2:330–43.
[32] Barkhordarian G, Klassen T, Bormann R. Fast hydrogen sorption kinetics of nanocrystalline Mg using Nb_2O_5 as catalyst. Scr Mater 2003;49:213–7.
[33] Borgschulte A, Bielmann M, Züttel A, Barkhordarian G, Dornheim M, Bormann R. Hydrogen dissociation on oxide covered MgH_2 by catalytically active vacancies. Appl Surf Sci 2008;254:2377–84.
[34] Friedrichs O, Sánchez-López JC, López-Cartes C, Klassen T, Bormann R, Fernández A. Nb_2O_5 "Pathway effect" on hydrogen sorption in Mg. J Phys Chem B 2006;110:7845–50.
[35] Montone A, Grbovic J, Bassetti A, Mirenghi L, Rotolo P, Bonetti E, et al. Microstructure, surface properties and hydrating behaviour of Mg–C composites prepared by ball milling with benzene. Int J Hydrogen Energy 2006;31:2088–96.
[36] Gutfleisch O, Dal Toe S, Herrich M, Handstein A, Pratt A. Hydrogen sorption properties of Mg–1 wt.% Ni–0.2 wt.% Pd

prepared by reactive milling. J Alloys Compd 2005;404–406:413–6.
[37] Czujko T, Varin RA, Chiu Ch, Wronski Z. Investigation of the hydrogen desorption properties of Mg + 10 wt.% X (X = V, Y, Zr) submicrocrystalline composites. J Alloys Compd 2006;414:240–7.
[38] Barkhordarian G, Klassen T, Bormann R. Kinetic investigation of the effect of milling time on the hydrogen sorption reaction of magnesium catalyzed with different Nb_2O_5 contents. J Alloys Compd 2006;407:249–55.
[39] Liang G, Huot J, Boily S, Van Neste A, Schulz R. Catalytic effect of transition metals on hydrogen sorption in nanocrystalline ball milled MgH_2–Tm (Tm = Ti, V, Mn, Fe and Ni) systems. J Alloys Compd 1999;292:247–52.
[40] Révész A, Fátay D, Spassov T. Hydriding kinetics of ball-milled nanocrystalline MgH_2 powders. J Mater Res 2007;22:3144–51.